Journal of Fluids and Structures (1999) **13,** 339–359
Article No.: jfls.1999.0206 available online at http://www.idealibrary.com on IDEAL

CHARACTERISTICS OF LOW-FREQUENCY VARIATIONS EMBEDDED IN VORTEX-SHEDDING PROCESS

J. J. Miau and J. T. Wang

Institute of Aeronautics and Astronautics, National Cheng Kung University Tainan, Taiwan 701, R.O.C.

J. H. Chou

Department of Engineering Science, National Cheng Kung University Tainan, Taiwan 701, R.O.C.

and

C. Y. Wei

Department of Aeronautics, Air Force Academy, Taiwan, R.O.C.

(Received 31 August 1997 and in revised form 13 November 1998)

Experiments were made to study the flow characteristics in the near-wake region of a two-dimensional bluff body, namely a trapezoidal cylinder (prism) or a circular cylinder. The instantaneous velocity signals obtained at the inner edge of the separated shear layer and in the neighbourhood of the rear end of the vortex formation region show the presence of low-frequency variations at Reynolds numbers of 10^4. The low-frequency variations noted in the velocity signals and the base pressure measured at the bluff body appear to be well correlated. These experimental observations suggest a physical picture that the variations of vortex formation length and base pressure are closely related in a real-time manner.

1. INTRODUCTION

Despite the flow characteristics of vortex shedding behind bluff bodies having been studied extensively for decades, the low-frequency variations embedded in the vortex-shedding process received little attention in the past. Among a few reports mentioning this characteristic of flow, Bloor (1964) first reported that for flow over a circular cylinder at Reynolds numbers in the transition range of 200–400, the velocity signals measured in the near-wake region showed an irregular appearance consisting of frequencies lower than the vortex-shedding frequency. Bloor (1964) suggested that these low-frequency variations are associated with the development of three dimensionality of the vortex-shedding structures. König *et al.* (1990) and Stäger & Eckelmann (1991) studied the effects of end-plates on vortex shedding from a circular cylinder at Reynolds numbers in the range of 10^2–10^3, showing that amplitude modulations in the velocity signals measured depend on the installation of end-plates. The vortex-shedding frequency measured in the region near the end-plate is different from that measured in the region away from the end-plate. Hence, an interaction of the two frequencies results in amplitude modulations.

0889–9746/99/040339 + 21 $30.00

Low-frequency variations were also noted in measurements of aerodynamic forces on a bluff body in cross-flow (Schewe 1983; Blackburn & Melbourne 1996; Lisoski 1993; Szepessy & Bearman 1992). Blackburn & Melbourne (1996) reported that a circular cylinder experienced low-frequency variations in lift in a free stream at turbulence level of 0·6% for Reynolds numbers of 10^5, but not so pronounced at higher turbulence levels. Schewe (1983) and Lisoski (1993) pointed out that low-frequency variations in drag and lift experienced by a bluff cylinder are in good correlation, which led further to the suggestion that the low-frequency variations seen are associated with the incoherence of vortex shedding in the spanwise direction. Experiments by Lisoski (1993) demonstrated that the characteristics of low-frequency modulations depend on the aspect ratio and on the presence of end-plates on the bluff cylinder. Szepessy & Bearman (1992) showed the existence of low-frequency modulations in pressure signals measured on a circular cylinder, which were explained as being due to an unsteady spanwise cellular structure in the shedding vortices. In a numerical study, Najjar & Balachandar (1997) showed that, for flow normal to a zero-thickness flat plate at $\mathrm{Re} = 250$, low-frequency unsteadiness is observed in the wake besides the primary shedding frequency during the vortex-shedding process, which led to the suggestion that the low-frequency unsteadiness might result from the transition between vortex shedding in the high- and the low-drag mode.

Miau *et al.* (1993) reported the finding of low-frequency variations embedded in the vortex-shedding signals measured at Reynolds numbers larger than 10^3. The laser-induced fluorescence flow visualization photographs presented in that study suggest that the low-frequency variations seen in the vortex-shedding process are associated with the unsteady variations of the vortex formation length. The linkage between the base pressure of a bluff body and the vortex formation length can also be seen in a number of reports which were concerned with the time-mean behavior mainly. Unal & Rockwell (1988) summarized the data reported by Bloor & Gerrard (1966), Gerrard (1978) and Blevins (1977) that the variations of the time-mean base pressure coefficient and vortex formation length of a circular cylinder are correlated for Reynolds numbers in a range of 10^2–10^5. The correlation indicates that as the base pressure gets larger, i.e. the base pressure coefficient gets less negative, the vortex formation length becomes longer.

It is the present authors' view that this behaviour can be explained as follows. The separated shear layers originating from the bluff body appear to have a curved shape, hence the centrifugal force associated with the curvature of the separated shear layer acts so as to balance the difference between the base pressure behind the bluff body and the pressure in the free stream. Therefore, as the base pressure increases, the separated shear layer takes on a flattened appearance and the vortex formation region becomes longer.

The relation between the base pressure and the vortex formation length can also be realized from a number of engineering applications. Wood (1964), Bearman (1967) and Tanner (1975) applied the base bleed technique to reduce the drag of aerodynamic bodies. This technique has an effect of increasing the base pressure, meanwhile lengthening the vortex formation region. Wong (1985) reported that introducing base bleed has the effect of stabilizing the wake oscillation behind a bluff body. As the bleed flow rate increases, the initial formation of vortices is delayed to further downstream, thus resulting in the suppression of vortex excitation of the bluff body. Bearman (1965) studied the wake characteristics of bluff bodies with blunt trailing edges and splitter plates. This report showed that by modifying the geometry of the bluff body the base pressure and the vortex formation length can be increased.

This work was motivated by a previous effort by Miau *et al.* (1993) concerning the development of a vortex flow meter for both liquid and gas flow-rate measurements. For a vortex flow meter, a sensor can be installed in the vortex-shedding bluff body, so as to

sense the pressure fluctuations associated with the vortex-shedding process. According to that previous study (Miau *et al.* 1993), the sensor signals obtained mainly consist of the vortex-shedding frequency and much lower frequencies components. The existence of the latter components apparently has an adverse effect, tending to degrade the quality of the signals obtained. While the signal quality can be improved by modifying the geometry of the bluff body (Miau *et al.* 1993), the presence of low-frequency fluctuations is noted as an intrinsic characteristic of vortex shedding which is worth being investigated in detail. Therefore, the present work is intended to study the relation between the base pressure and the vortex formation length with regard to the low-frequency variations observed.

2. EXPERIMENTAL METHOD

Experiments were conducted in a low-speed wind tunnel with a square test-section 150 mm by 150 mm. The turbulence level measured in the test-section was about 0·6% at the mean velocity of 14 m/s. The two-dimensional bluff bodies employed were a trapezodial cylinder and a circular cylinder. The trapezoidal cylinder was installed with the wider side facing the incoming flow whose width, D, was 32 mm. The diameter of the circular cylinder employed was also 32 mm. Therefore, the blockage ratio based on the frontal area of either of the bluff bodies was about 21%. Each of the bluff bodies were mounted in the test-section between the side walls, where the boundary-layer thickness measured was about 0·4 D

Experiments were performed at a Reynolds number of 10^4. The Reynolds number, denoted by Re, is defined based on the characteristic velocity of the free stream, U^*, and the width of the bluff body, D; U^* is the free-stream velocity around the bluff body, for which blockage has been taken into account.

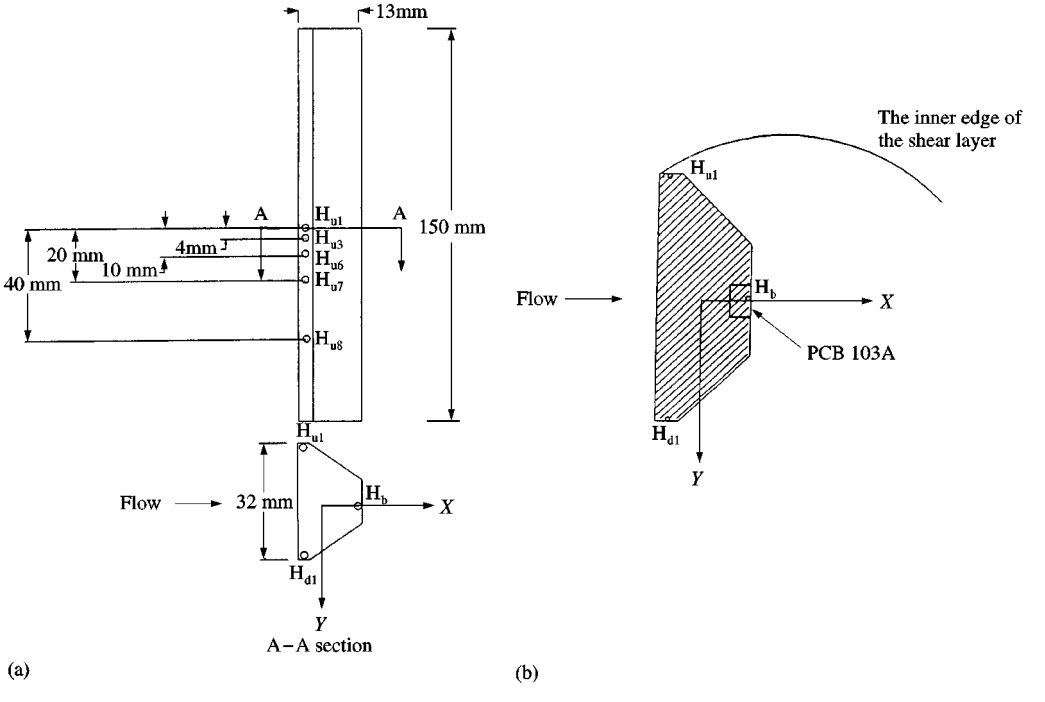

Figure 1. Schematic drawings of the trapezoidal cylinder (a) with the pressure taps, and (b) with the piezoelectric pressure sensor.

Pressure taps of 1 mm in diameter were provided on the rear surfaces of the bluff bodies as seen in Figures 1 and 2. These pressure taps allowed for pressure measurements at the mid-span of the bluff body as well as along the spanwise direction. Diaphragm-type pressure transducers, Validyne DP-103, were employed for acquiring the pressure variations at the pressure taps, and subsequently for correlation measurements. As will be seen later, these diaphragm-type pressure transducers had a deficiency in measuring the response of the instantaneous pressure fluctuations around the bluff body. Alternatively, a piezoelectric pressure transducer, PCB 103 A, was employed for instantaneous base-pressure measurements. This pressure sensor was installed on the rear face of the trapezoidal cylinder as shown in Figure 1(b).

For the instantaneous velocity measurements in the separated shear layers downstream of the bluff body, a single normal hot-wire probe was employed. Further, in order to obtain the instantaneous velocity fluctuations in the neighbourhood of the rear end of the vortex formation region, a split fibre probe was employed. This probe was capable of

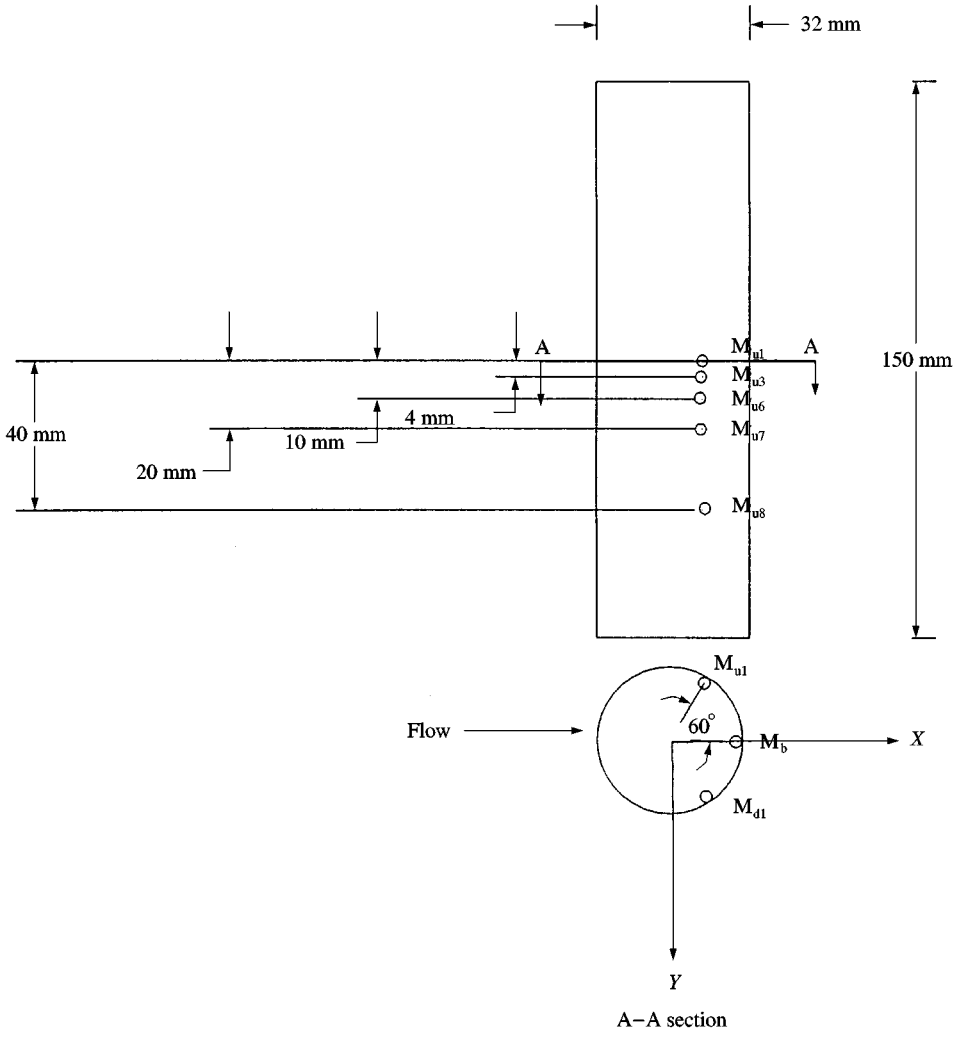

Figure 2. A schematic drawing of the circular cylinder with the pressure taps.

differentiating the forward and reverse velocities in the streamwise direction. In this work, the rear end of the vortex formation region was referred to the location where the probabilities of streamwise velocity in the forward and reverse directions measured are equal, by reasoning that in the time-mean sense the vortex formation region is enclosed by a free streamline. In the literature, for instance, Szepessy & Bearman (1992), the vortex formation position is frequently determined as the location where the fluctuating signal output by a hot wire reaches a peak value, reflecting the fact that flow is highly unsteady at this position. The difference between the vortex formation lengths deduced by the two methods described above was not pursued further, since the exact vortex formation length was not of major concern in this work.

The coordinate system employed for the present study is described in Figures 1 and 2 for the cases of the trapezoidal and the circular cylinder, respectively. X denotes the streamwise axis, with the positive direction pointing downstream. Y denotes the vertical axis, positive downward, and Z denotes the spanwise axis. The origin, $X = 0$, $Y = 0$ and $Z = 0$, is located at the geometrical centre of the bluff body.

3. RESULTS AND DISCUSSION

3.1. The Case of Flow over a Trapezoidal Cylinder

Correlation of the base-pressure fluctuations and the velocity fluctuations measured in the separated shear layer was examined first. The velocity measurements were made at the location A, located at the inner edge of the separated layer, shown in Figure 3(a). At this location, the low-frequency variations could be clearly detected, whereas further toward the region of strong transverse shear fluctuations measured were dominated by higher-frequency components. In Figure 3(b), the three signal traces of base pressure measured at the pressure taps H_b, H_{u1}, and H_{d1}, and a velocity signal trace obtained at the location A at $Re = 2{\cdot}7 \times 10^4$ are presented. The pressure data are expressed in terms of the nondimensional coefficient C_p, and the instantaneous velocity data are normalized by the characteristics velocity as u/U^*. Here, C_p is defined as

$$C_p = \frac{p - p_r}{\frac{1}{2}\rho U^{*2}}, \tag{1}$$

where p is the instantaneous pressure measured, p_r denotes the reference pressure which was measured on the wall 12D upstream of the bluff body, and ρ denotes the density of the fluid.

In Figure 3(b), the pressure-signal traces and the velocity-signal traces show a common feature that low-frequency variations are significantly present. Further, the low-frequency variations appear to be of a time scale comparable to or even larger than $10T_s$, where T_s denotes the characteristic time period of vortex shedding. Hence, it is reasonable to state that the low-frequency component seen can easily be separated from the vortex-shedding frequency component by a conventional filtering technique. The low-frequency variations embedded in the velocity signal imply that the separated shear layer is in a flapping motion. To be more specific, as the separated shear layer moves outward, the hot-wire probe at a fixed position experiences lower velocity. Conversely, as the separated shear layer moves inward, the hot-wire probe senses strong velocity fluctuations in the shear layer. Such a behaviour was also noted in the occurrence of a turbulent separation bubble on a flat plate (Kiya & Sasaki 1983) and the plane jet flow (Goldschmidt 1973).

The low-frequency variations embedded in the pressure-signal and the velocity-signal traces shown in Figure 3(b) are further examined in Figure 3(c). The traces shown are the result of low-pass filtering of the signal traces in Figure 3(b), with a cut-off frequency at 5 Hz.

The cut-off frequency chosen was based on the fact that, for the present flow, the low-frequency variations were mainly confined below 5 Hz, while the vortex-shedding frequency was about 40 Hz. This cut-off frequency was adopted for all the cases reported in the paper. Correlations are presented in terms of the time-lag correlation coefficient $R_L(q_1, q_2, \tau)$, defined by

$$R_L(q_1, q_2, \tau) = \frac{\overline{q_1(t)q_2(t+\tau)}}{(\overline{q_1^2})^{1/2}(\overline{q_2^2})^{1/2}}. \tag{2}$$

The subscript L signifies that the correlation is for the low-pass filtered traces of q_1 and q_2. The symbols of q_1 and q_2 represent the instantaneous values of the quantities $C_p(\mathrm{H_b})$,

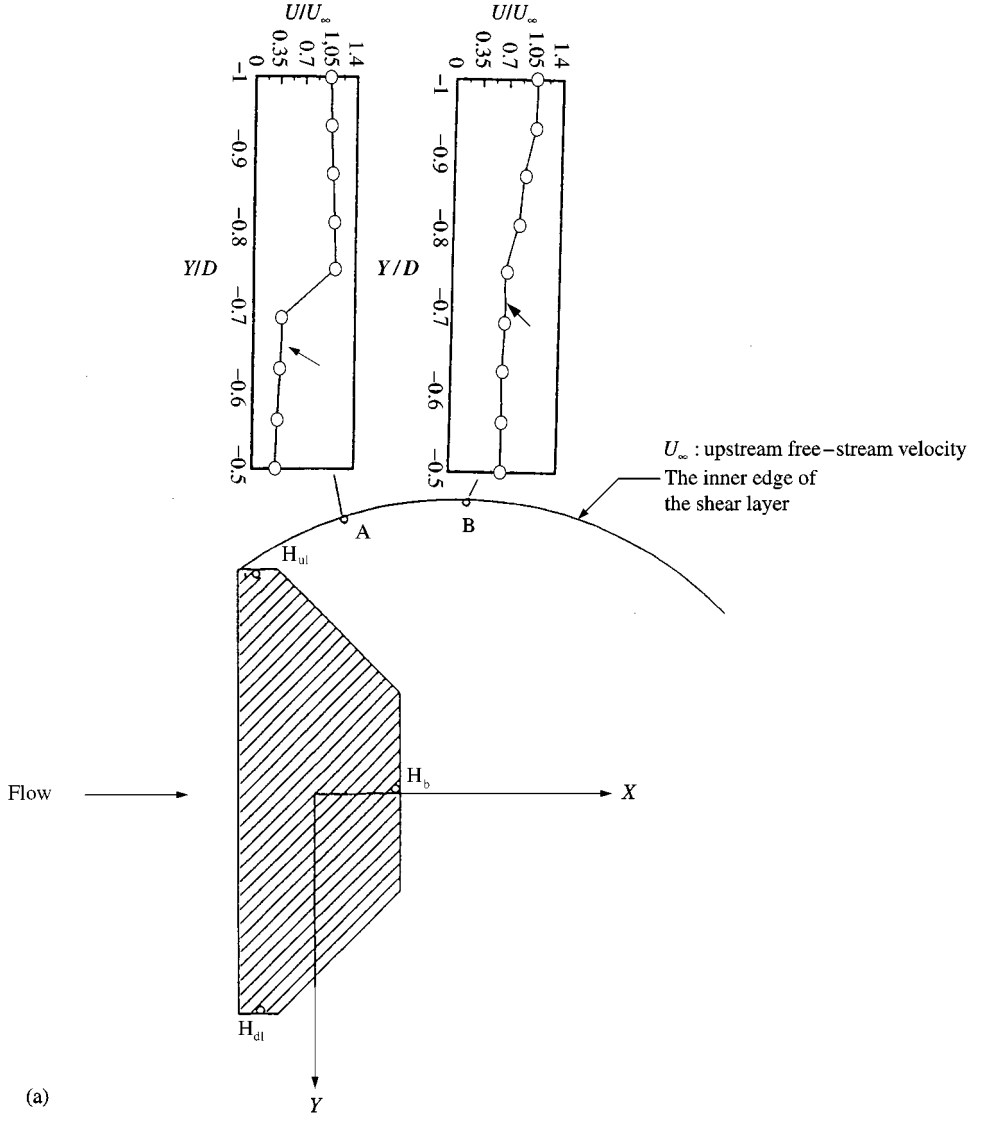

Figure 3(a). A schematic drawing of a trapezoidal cylinder and points A and B situated at the inner edge of the separated shear layer where the instantaneous velocity measurements were performed.

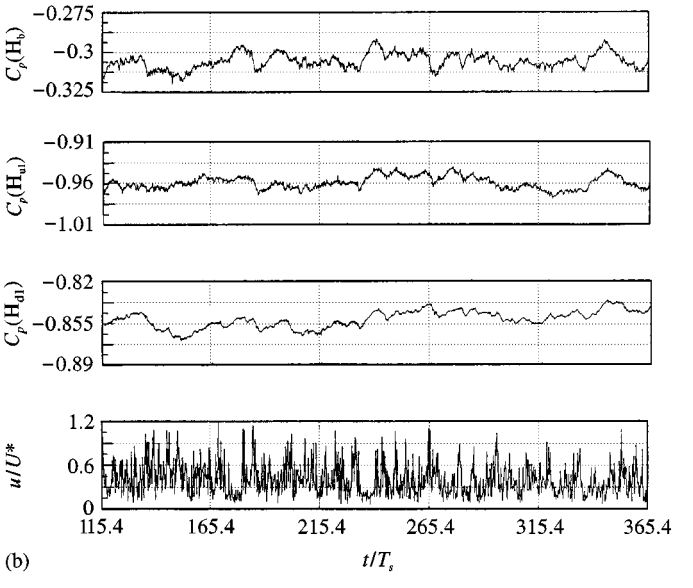

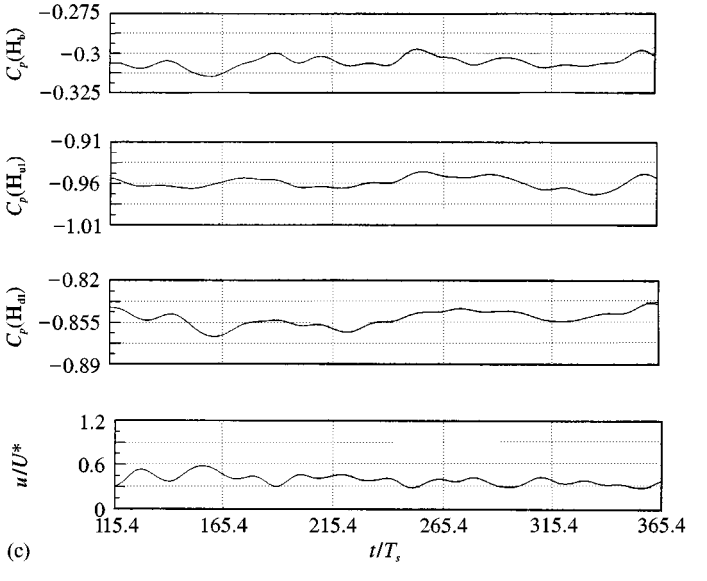

Figure 3. (b) The pressure-signal traces of $C_p(H_b)$, $C_p(H_{u1})$, and $C_p(H_{d1})$, and the velocity signal trace of u/U^* obtained at the point A, i.e. $X/D = 0{\cdot}094$ and $Y/D = -0{\cdot}6875$, at $Re = 2{\cdot}7 \times 10^4$. (c) The low-pass filtered traces corresponding to those shown in Figure 3(b).

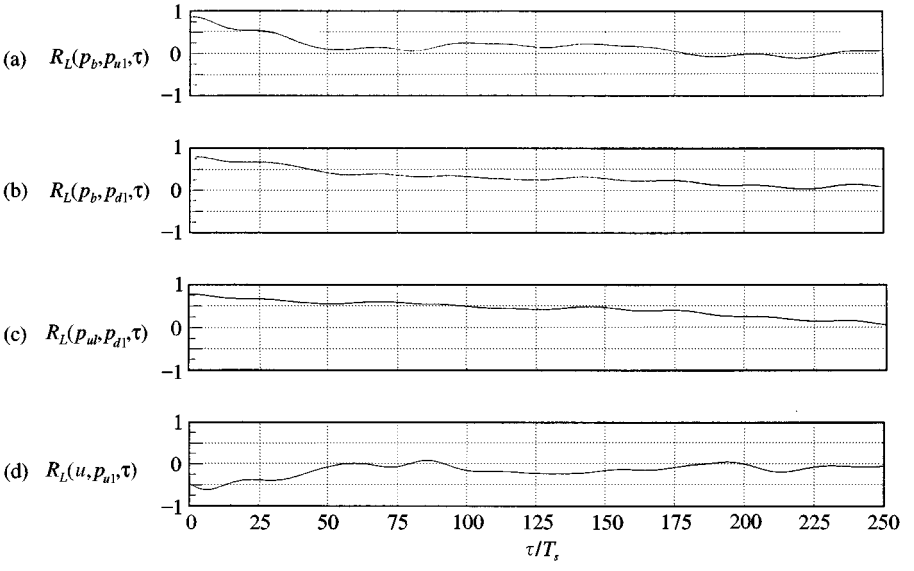

Figure 4. Plots of (a) $R_L(p_b, p_{u1}, \tau)$, (b) $R_L(p_b, p_{d1}, \tau)$, (c) $R_L(p_{u1}, p_{d1}, \tau)$, and (d) $R_L(u, p_{u1}, \tau)$ for the signal traces shown in Figure 3(c).

$C_p(\mathrm{H_{u1}})$, $C_p(\mathrm{H_{d1}})$ and u/U^*, which are abbreviated as p_b, p_{u1}, p_{d1} and u, respectively, for later usage; τ denotes the time lag between the quantities of q_1 and q_2. The results of $R_L(p_b, p_{u1}, \tau)$, $R_L(p_b, p_{d1}, \tau)$, $R_L(p_{u1}, p_{d1}, \tau)$ and $R_L(u, p_{u1}, \tau)$ are shown in Figure 4(a,b,c,d). It is first noted that, in Figure 4(a,b,c) the values of $R_L(p_b, p_{u1}, \tau)$, $R_L(p_b, p_{d1}, \tau)$, and $R_L(p_{u1}, p_{d1}, \tau)$ at $\tau = 0$ are higher than 0·75, suggesting that the low-frequency variations detected at the pressure taps at the mid-span of the bluff body are essentially in phase. Second, as seen in Figure 4(d), the value of $R_L(u, p_{u1}, \tau)$ at $\tau = 0$ is negative, and about $-0{\cdot}5$; this implies that the low-frequency variations in the base-pressure and the velocity-signals measured are correlated in an out-of-phase manner. The occurrence of the most negative value of $R_L(u, p_{u1}, \tau)$ at $\tau = 5T_s$, not at $\tau = 0$, is noted; this is essentially due to the time-lag response of the diaphragm pressure transducer employed which will be discussed later.

More hot-wire velocity measurements were made at a number of locations in the separated shear layer for studying the evolution of the low-frequency variations in the streamwise direction. As an example, the velocity-signal obtained at location B in Figure 3(a), and the base-pressure signal obtained simultaneously are shown in Figure 5(a). The low-pass filtered traces and their time-lag correlation plots are given in Figure 5(b,c). Figure 5 shows similar characteristics to those seen in Figures 3 and 4 described previously.

As the hot-wire probe moves further downstream, the low-frequency variations in the velocity signals measured becomes less obvious, because the velocity fluctuations become dominated by the vortex-shedding frequency and higher-frequency components. In general, the characteristic of low-frequency variations can be clearly detected by the hot-wire in the region of $X/D < 1{\cdot}5$, at the inner edge of the separated shear layer.

The above findings of low-frequency variations in the base pressure and the instantaneous velocity in the separated shear layers measured encouraged the authors to study further the unsteady characteristics associated with the vortex formation region. The velocity measurements in the neighbourhood of the rear end of the vertex formation region were conducted by a split fibre probe.

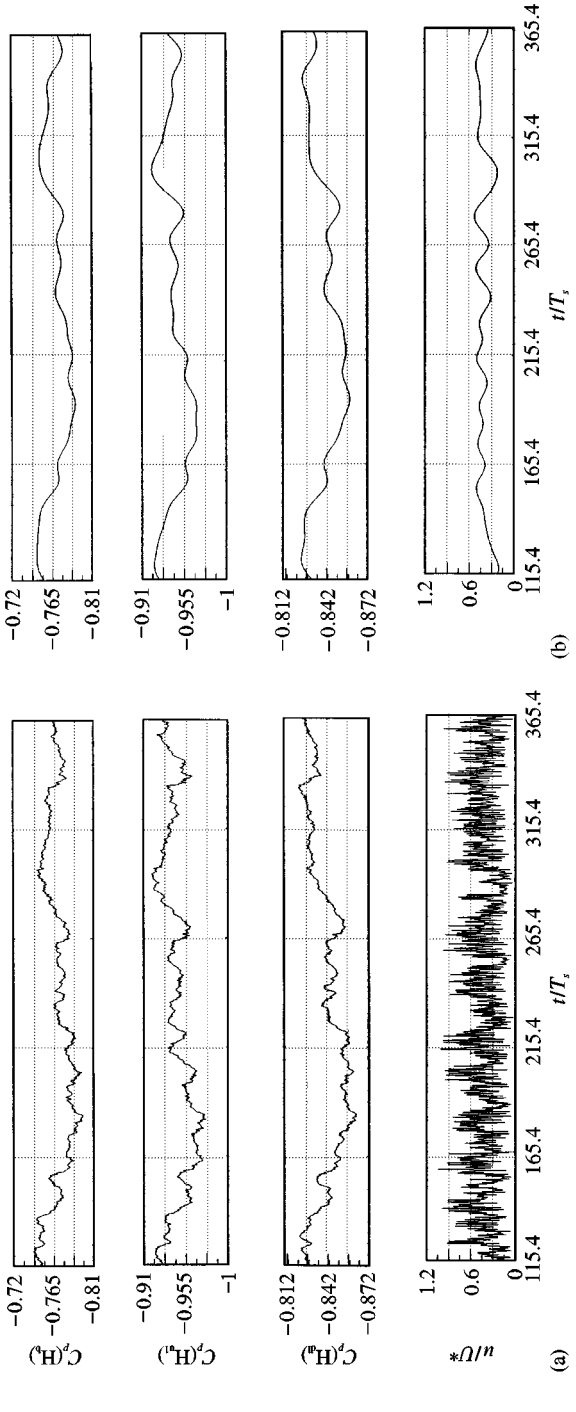

Figure 5. (a) The pressure signal traces of $C_p(H_b)$, $C_p(H_{u1})$, and $C_p(H_{d1})$, and the velocity signal trace of u/U^* obtained at the point B, i.e. $X/D = 0{\cdot}844$ and $Y/D = -0.719$, at $Re = 2.7 \times 10^4$. (b) The low-pass filtered traces corresponding to those shown in (a).

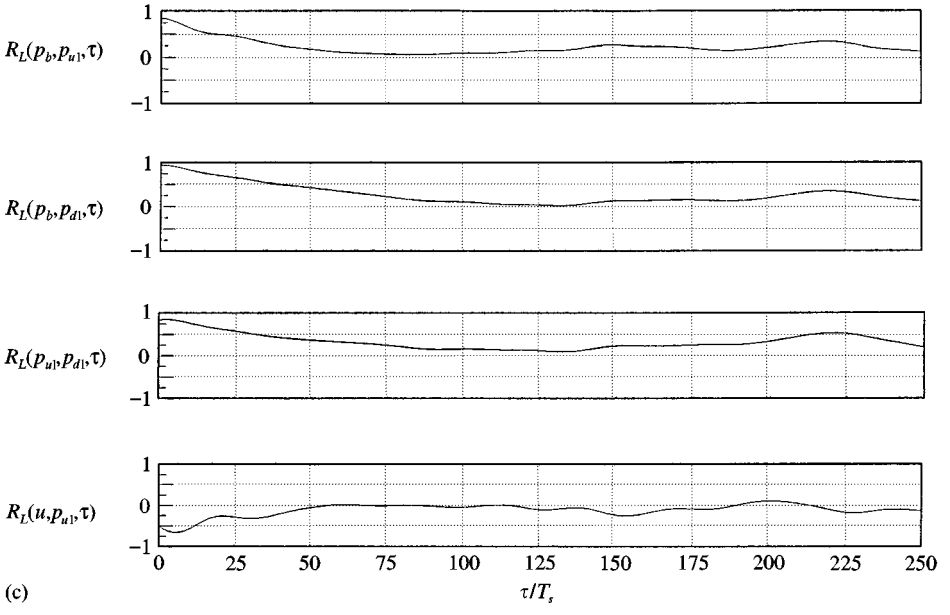

Figure 5 (c). Plots of $R_L(p_b, p_{u1}, \tau)$, $R_L(p_b, p_{d1}, \tau)$, $R_L(p_{u1}, p_{d1}, \tau)$, and R_L (u, p_{u1}, τ) for the signal traces shown in Figure 5(b).

Figures 6(a) and 6(b) present the results for the split fibre probe located at (a) $X/D = 1{\cdot}575$ and $Y/D = 0$ for $\mathrm{Re} = 3{\cdot}3 \times 10^4$, and (b) $X/D = 2{\cdot}043$ and $Y/D = 0$ for $\mathrm{Re} = 2{\cdot}7 \times 10^4$, respectively. It should be mentioned that the two streamwise locations chosen were situated upstream and downstream of the rear end of the vortex formation region, respectively. Both of Figure 6(a) and 6(b) show evidence of low frequency variations in the signal traces of $C_p(\mathrm{H_b})$ and u/U^*. The traces of u/U^* reveal that the instantaneous velocities measured are fluctuating between positive and negative values, which is a characteristic of the flow in the neighborhood of the rear end of the vortex formation region. The low-frequency variations in base pressure and velocity measured are correlated in an out-of-phase manner roughly speaking. This can be further realized from Figure 7, which presents the time-lag correlation results of the low-pass filtered traces. In both plots of Figure 7 the values of $R_L(u, p_{u1}, 0)$ are seen to be negative, while the most negative values occurred at $\tau = 0{\cdot}15$ s in physical time. Hence, it is revealed from the data shown in Figures 6 and 7 that the low-frequency variations in the instantaneous velocity measured in the neighborhood of the vortex formation position are in good correlation with the low-frequency variations seen in the pressure signals obtained on the rear surface of the cylinder. It should be mentioned that no further effort was made to find the streamwise location of the split fibre corresponding to where the maximum negative value of $R_L(u, p_{u1}, \tau)$ occurred.

The appearance of the most negative correlation coefficients of $R(u, p_{u1}, \tau)$ at $\tau \neq 0$ in Figures 7 and 4(d) is attributed to the problem of the diaphragm-type pressure sensor employed. This problem was confirmed by the experiments using the piezoelectric sensors instead, for base-pressure measurements. By having a piezoelectric pressure transducer installed at the location $\mathrm{H_b}$, the signal traces obtained at $\mathrm{Re} = 2{\cdot}7 \times 10^4$ and $3{\cdot}1 \times 10^4$ are shown in Figures 8(a,b). In the figures, the signal traces obtained by the split fibre positioned at $X/D = 1{\cdot}77$, $Y/D = 0$ are also given. Figure 9 presents the time-lag correlation plots of the low-pass filtered traces corresponding to those shown in Figure 8. It is seen that the most negative correlation coefficients in these plots occur at $\tau = 0$, unlike those seen in

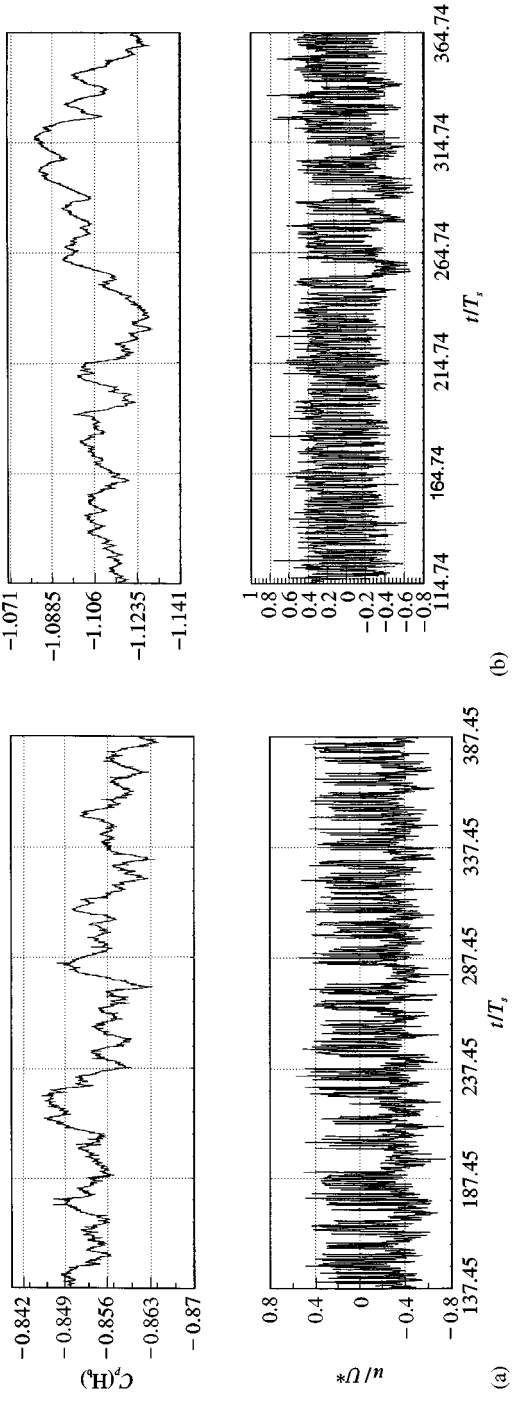

Figure 6. (a) The pressure signal trace of $C_p(H_b)$ and the velocity signal trace u/U^* obtained at $X/D = 1{\cdot}575$ and $Y/D = 0$, at $Re = 3{\cdot}3 \times 10^4$. (b) The pressure signal trace of $C_p(H_b)$ obtained by the diaphragm-type pressure transducer and the velocity signal trace of u/U^* obtained by the split fiber probe at $X/D = 2{\cdot}043$ $Y/D = 0$, $Re = 2{\cdot}7 \times 10^4$.

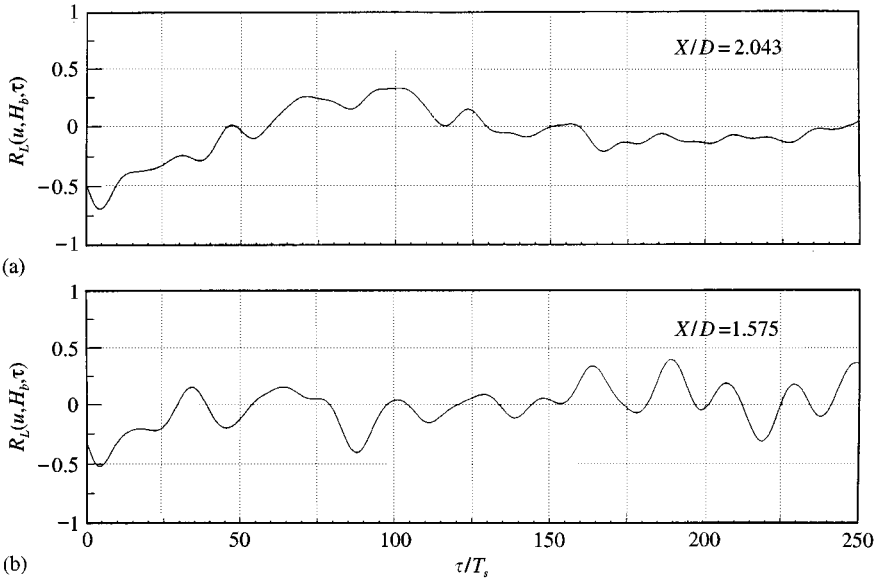

Figure 7. Plots of the time-lag correlation coefficients for (a) the low-pass filtered traces corresponding to those shown in Figure 6(a), and (b) the low-pass filtered traces corresponding to those shown in Figure 6(b).

Figures 7 and 4(d). This finding has the further implication that the low-frequency variations seen in the base-pressure fluctuations and the velocity fluctuations develop in an instantaneous fashion. Also noted from a comparison of the raw pressure signals of Figures 8 and 5 is that the piezoelectric pressure sensor displays a better response to fluctuations of high frequency. It is also noted in Figures 7(b) and 9(b) that the correlation distributions of $R_L(u, p_{u1}, \tau)$ do not fall to zero at large τ. Intuitively, one knows that the correlation coefficients of $R_L(u, p_{u1}, \tau)$ should go to zero for large τ. This is true for most of the time-lag correlation distributions shown in this paper, except for Figures 7(b) and 9(b). No explanation for the appearance of Figures 7(b) and 9(b) can be given at present.

The experimental observations reported above suffice for proposing a physical picture regarding the presence of low-frequency variations in the near-wake region. A schematic in Figure 10(a) shows that, as the base pressure is increased, the separated shear layer tends to move outward; thus the streamwise extent of the vortex formation region is enlarged. Similarly, the schematic in Figure 10(b) describes the reverse situation. These sketches, it is noted, are consistent with the flow visualization photographs by Miau *et al.* (1993), as well as the pressure–velocity correlation results presented in this paper. Hence, the flapping motions of the separated shear layers discussed previously are actually associated with the unsteady variations of the vortex formation length. A picture emerging from a combination of Figures 10(a) and 10(b) is that the vortex formation region varies in size with respect to time. These variations are of a time scale one order of magnitude larger than the time scale of vortex shedding. It should be noted that although the hot-wire velocity measurements presented in this paper were made in the separated shear layer on one side of the trapezoidal cylinder, the characteristics of the separated shear layer on the other side can be deduced automatically, based on the argument of symmetry of this flow configuration.

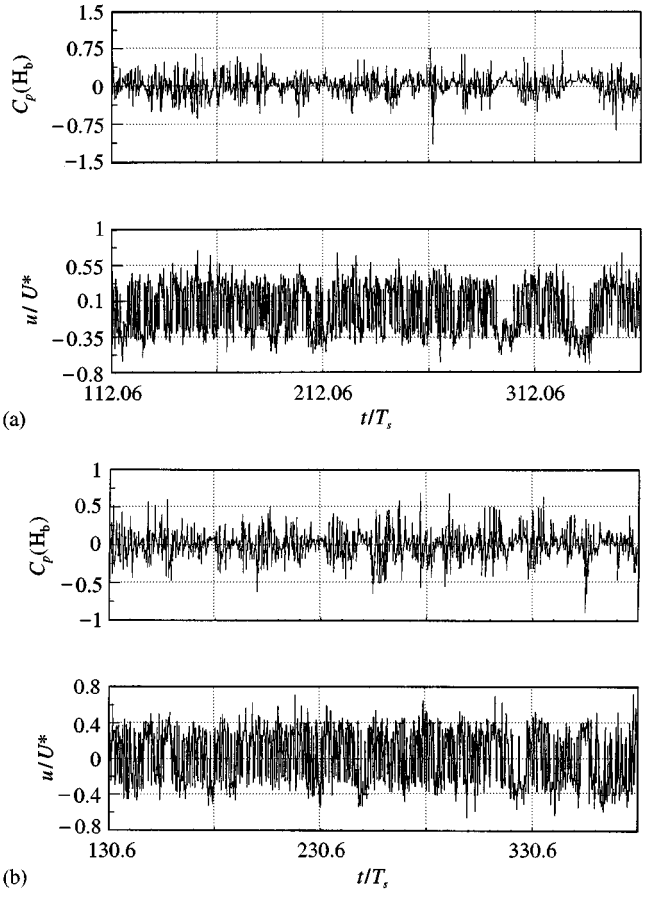

Figure 8. The pressure signal traces of $C_p(H_b)$ obtained by the piezoelectric pressure transducer and the velocity signal traces of u/U^* obtained by the split fibre probe, at $X/D = 1{\cdot}77$ and $Y/D = 0$, (a) for $Re = 2{\cdot}7 \times 10^4$, and (b) for $Re = 3{\cdot}2 \times 10^4$.

The spanwise characteristics of the low-frequency variations are also of interest in the present study. Figures 11(a) and 11(b) present the signal traces obtained by three diaphragm-type pressure transducers at the pressure taps H_{u1}, H_{u3}, and H_{u6}, and at H_{u1}, H_{u7}, and H_{u8}, respectively, for $Re = 3{\cdot}3 \times 10^4$; refer to Figure 1 for the physical locations of the pressure taps mentioned. The plots of $R_L(p_{u1}, p_{u3}, \tau)$, $R_L(p_{u1}, p_{u6}, \tau)$, $R_L(p_{u1}, p_{u7}, \tau)$ and $R_L(p_{u1}, p_{u8}, \tau)$ are given in Figure 11(c). Although the diaphragm-type pressure transducers employed have a deficiency in the delay of response to pressure fluctuations, the correlation results presented in Figure 11(c) do not show this problem because the time lag effects of the pressure transducers are canceled out in the correlation. As seen in these plots, the maximum correlation coefficients occur at $\tau = 0$, which remain above 0·9 even for the largest separation of $1{\cdot}25D$ between the pressure taps H_{u1} and H_{u8}. These findings strongly imply that the spanwise integral length scale of the low-frequency variations is much larger than the characteristic length scale of the bluff body which is D. This finding is consistent with previous experimental and numerical studies (Szepessy & Bearman 1992; Lisoski 1993; Henderson 1997).

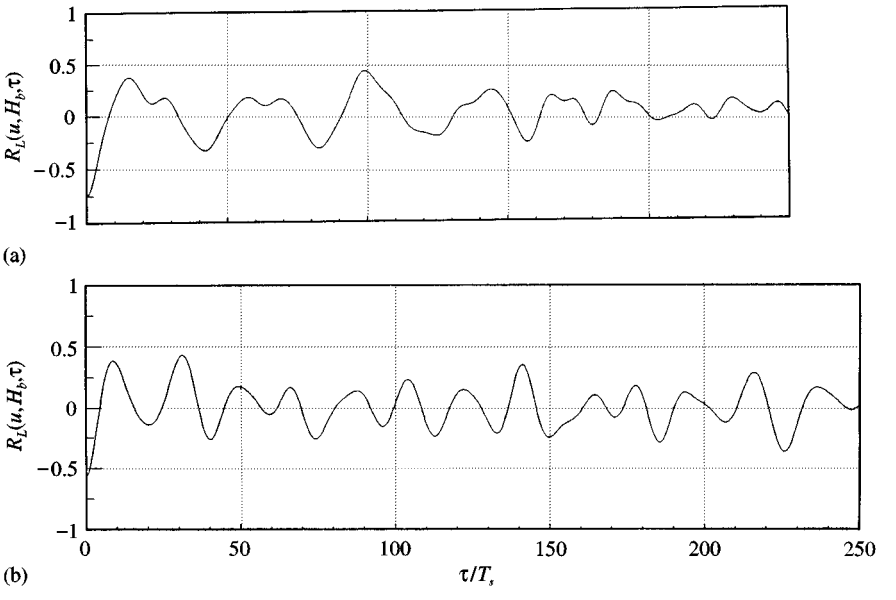

Figure 9. Plots of the time-lag correlation coefficients for (a) the low-pass filtered traces corresponding to those shown in Figure 8(a), and (b) the low-pass filtered traces corresponding to those shown in Figure 8(b).

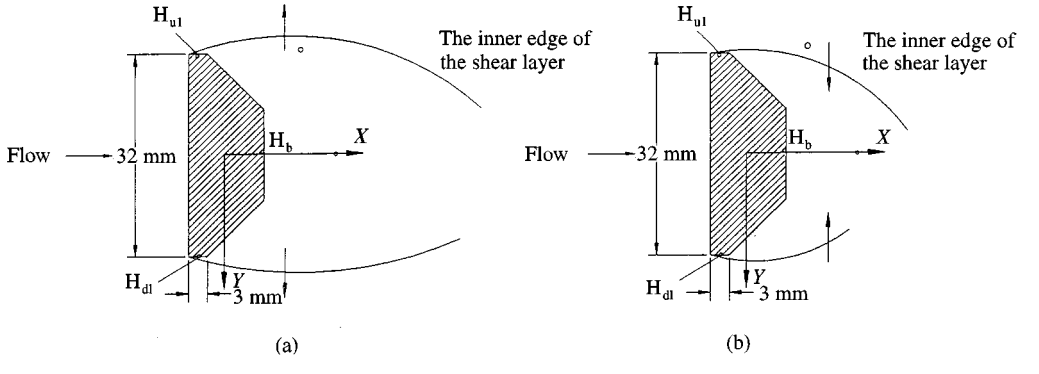

Figure 10. A physical model concerning the variations of the base pressure and the vortex formation length. (a) The situation when the base pressure is relatively large; (b) the situation when the base pressure is relatively small.

3.2. The Case of Flow over a Circular Cylinder

Further experiments were made for flow over the circular cylinder, to examine whether the low-frequency variations prevail in vortex shedding or not. Figure 12(a) shows point A, at $X/D = 0{\cdot}844$, $Y/D = -0{\cdot}7187$ and $Z = 0$, near the inner edge of the separated shear layer which was selected for detecting the instantaneous velocity fluctuations. Figure 12(b) presents the velocity signals obtained by a single normal hot wire at $\mathrm{Re} = 2{\cdot}7 \times 10^4$ together with the base-pressure traces obtained at the pressure taps M_b, M_{u1}, and M_{d1} by three diaphragm-type pressure transducers. Correspondingly, the plots of $R_L(p_b, p_{u1}, \tau)$, $R_L(p_b, p_{d1}, \tau)$, $R_L(p_{u1}, p_{d1}, \tau)$ and $R_L(u, p_{u1}, \tau)$ are given in Figure 12(c). A comparison of

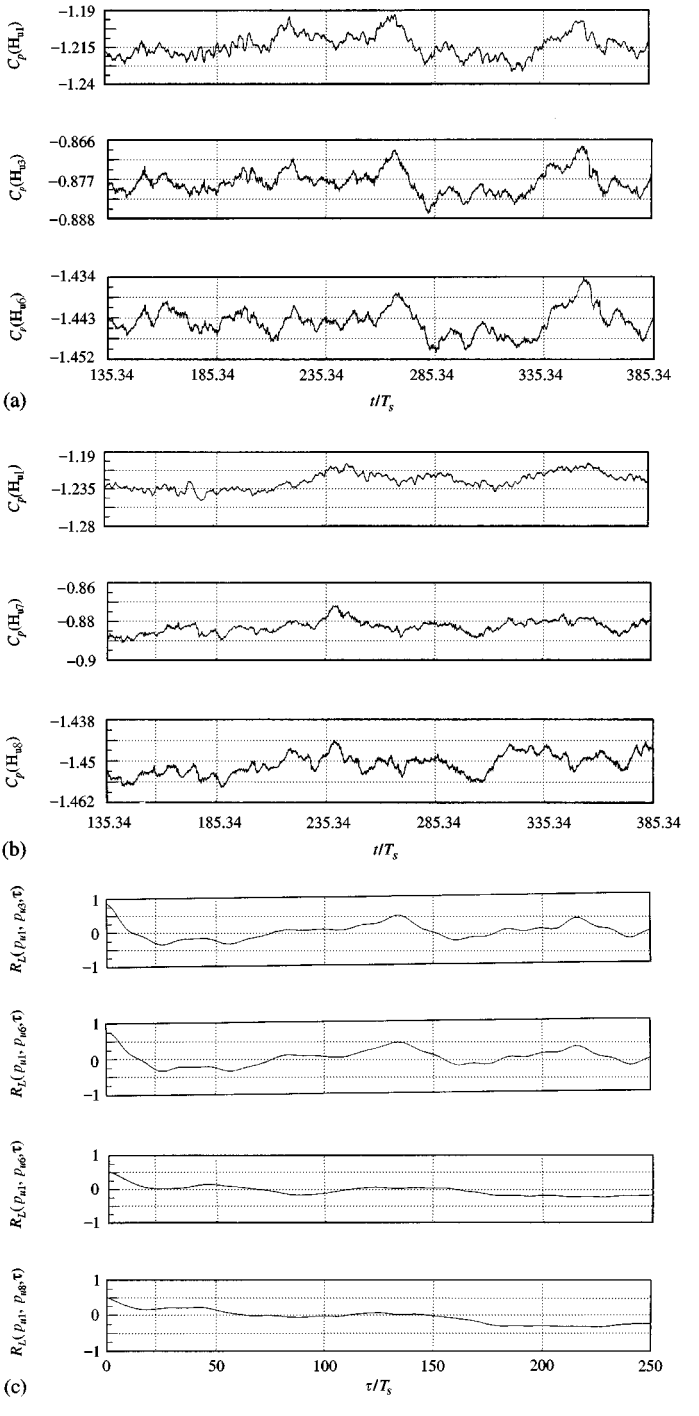

Figure 11. (a) The instantaneous pressure-signal traces obtained at the pressure taps H_{u1}, H_{u3}, and H_{u6} on the trapezoidal cylinder at $Re = 3{\cdot}3 \times 10^4$. (b) The instantaneous pressure-signal traces obtained at the pressure taps (a) H_{u1}, H_{u7}, and H_{u8} on the trapezoidal cylinder at $Re = 3{\cdot}3 \times 10^4$. (c) Plots of $R_L(p_{u1}, p_{u3}, \tau)$, $R_L(p_{u2}, p_{u6}, \tau)$, $R_L(p_{u1}, p_{u7}, \tau)$, $R_L(p_{u1}, p_{u8}, \tau)$ for the signal traces shown in (a) and (b).

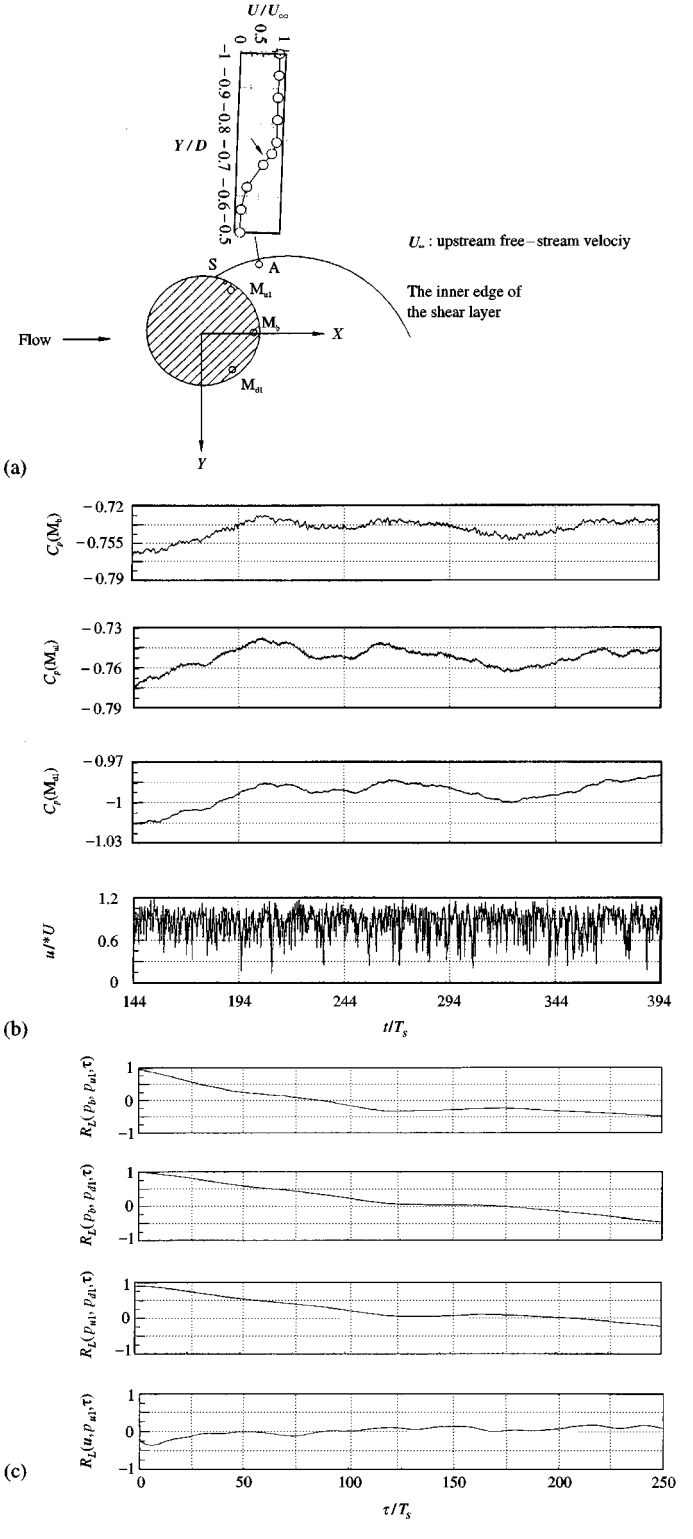

Figure 12. (a) A schematic drawing of the circular cylinder and the point A situated at the inner edge of the separated shear layer where the instantaneous velocity measurements were performed. (b) The pressure-signal traces of $C_p(M_b)$, $C_p(M_{u1})$, and $C_p(M_{d1})$ and the velocity signal trace of u/U^* obtained at point A, i.e. $X/D = 0{\cdot}844$ and $Y/D = -0{\cdot}7187$, at $Re = 2{\cdot}7 \times 10^4$. (c) Plots of $R_L(p_b, p_{u1}, \tau)$, $R_L(p_b, p_{d1}, \tau)$, $R_L(p_{u1}, p_{d1}, \tau)$, $R_L(u, p_{u1}, \tau)$ for the signal traces shown in (b).

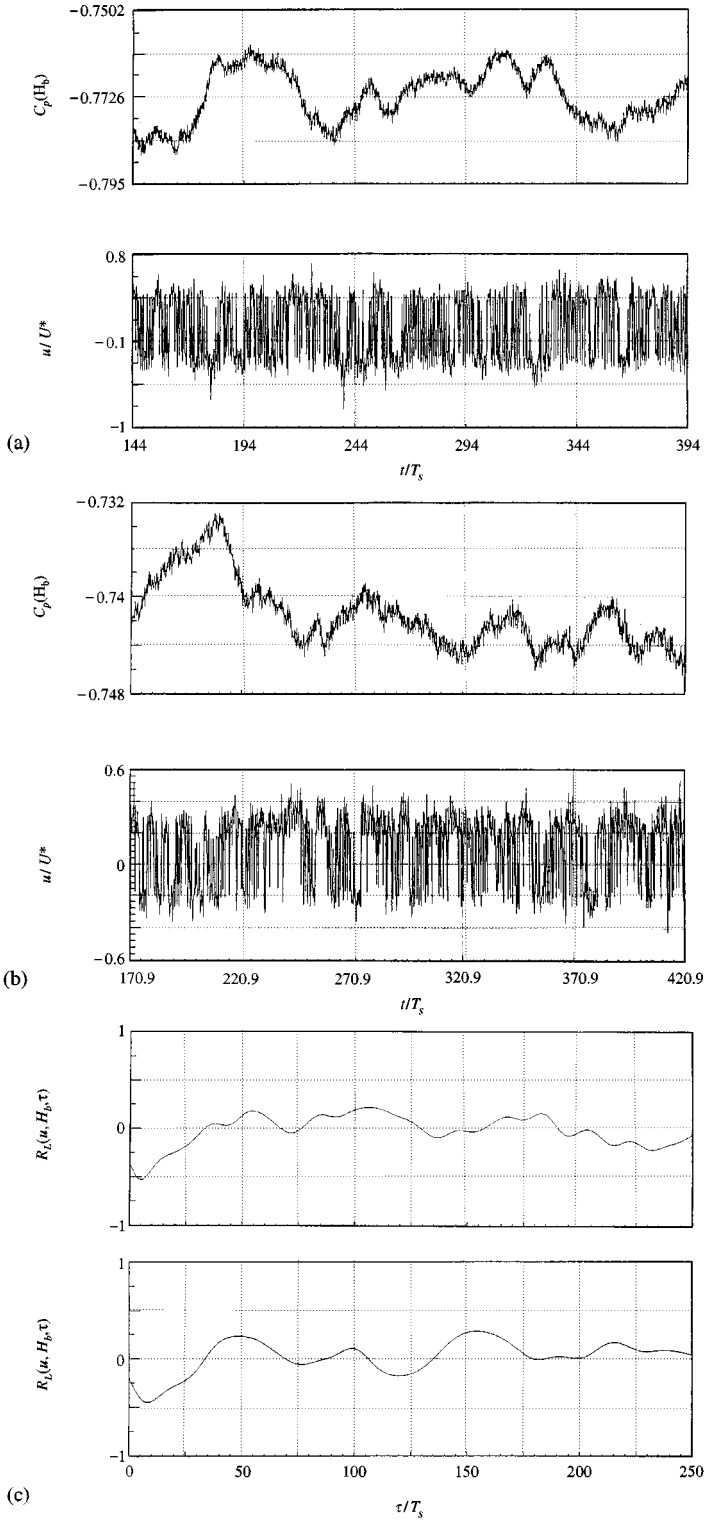

Figure 13. The pressure-signal traces of $C_p(H_b)$ obtained by the diaphragm-type pressure transducer and the velocity signal traces of u/U^* obtained by the split fibre probe at (a) $X/D = 2{\cdot}53$ and $Y/D = 0$, at $\mathrm{Re} = 2{\cdot}7 \times 10^4$, and (b) at $X/D = 2{\cdot}31$ and $Y/D = 0$, for $\mathrm{Re} = 3{\cdot}3 \times 10^4$. (c) Plots of the time-lag correlation coefficients of the low-pass filtered traces corresponding to those shown in (a) and (b).

Figure 12 and Figures 3–5 indicates that the characteristics of low-frequency variations in the two cases, for flow over the trapezoidal cylinder and a circular cylinder, are similar. Notable features obtained from Figure 12 are summarized as follows.

(i) The presence of low-frequency variations is confirmed by the base-pressure and velocity traces presented in Figure 12(b).

(ii) The low-frequency variations detected at the three pressure taps on the rear surface of the cylinder at mid-span tend to be in phase, as shown in Figures 12(b).

(iii) The low-frequency variations embedded in the velocity fluctuations and the base-pressure fluctuations tend to be out-of-phase. The appearance of nonzero time lag associated with the most negative correlation coefficient obtained is again attributed to the dynamic response of the diaphragm-type pressure transducer.

The velocity fluctuations obtained by the split fibre probe in the neighbourhood of the rear end of vortex formation region are shown in Figures 13(a) and 13(b), i.e. the signal traces obtained at (a) $X/D = 2{\cdot}53$ and $Y/D = 0$, for $\mathrm{Re} = 2{\cdot}7 \times 10^4$ and (b) $X/D = 2{\cdot}31$ and $Y/D = 0$ for $\mathrm{Re} = 3{\cdot}3 \times 10^4$. In these two figures, the instantaneous base-pressure fluctuations obtained by the diaphragm-type pressure transducer at the pressure tap $\mathrm{M_b}$ are also presented. Figure 13(c) gives two plots of $R_L(u, p_b, \tau)$ associated with the signal traces shown in Figure 13(a) and 13(b) respectively. The correlation coefficients of $R_L(u, p_b, 0)$ are negative and comparable to those reported previously for the case of flow over a trapezoidal cylinder. Therefore, the physical model of Figure 10 is applicable for explaining the measurement results of Figures 12 and 13.

The pressure signal traces obtained at the pressure taps along the spanwise direction on the circular cylinder are presented in Figures 14(a) and 14(b). Correspondingly, the time-lag correlation plots corresponding to the low-pass filtered traces are given in Figure 14(c). It is seen in Figure 14(c) that the correlation coefficients at $\tau = 0$ are even higher than those seen in the previous case of flow over the trapezoidal cylinder. Thus, the low-frequency variations seen in the vortex-shedding process maintain high correlation along the span of the cylinder.

4. CONCLUDING REMARKS

The experimental results obtained in this study lead to the following conclusions.

1. The presence of low-frequency variations in the vortex-shedding process is confirmed in the two cases of flow over a trapezoidal cylinder and flow over a circular cylinder at Reynolds numbers above 10^4.

2. The experimental results obtained suffice to draw a physical picture that the low-frequency variations embedded in the base pressure and the velocity fluctuations measured in the near-wake region are correlated in a real-time manner. As the base pressure is increased, the vortex formation region is lengthened, and *vice versa*. These variations are of a time scale one order of magnitude larger than the characteristic time scale of vortex shedding.

3. The low-frequency variations measured are in high correlation along the span of the cylinder.

Further remarks concerning future work are as follows. Evidence from the literature (Lisoski 1993; Szepessy & Bearman 1992; Blackburn & Melbourne 1996) indicates that the characteristics of low-frequency variations in vortex shedding are sensitive to aspect ratio, Reynolds number, end-plates on the cylinder and free-stream turbulence. Since the present experiments were made specifically for bluff cylinders of aspect ratio 4·7, spanning the walls of the test-section, at a Reynolds number of 10^4 and with free-stream turbulence level of 0·6%, more effort is necessary in the future to study the influence of these parameters systematically.

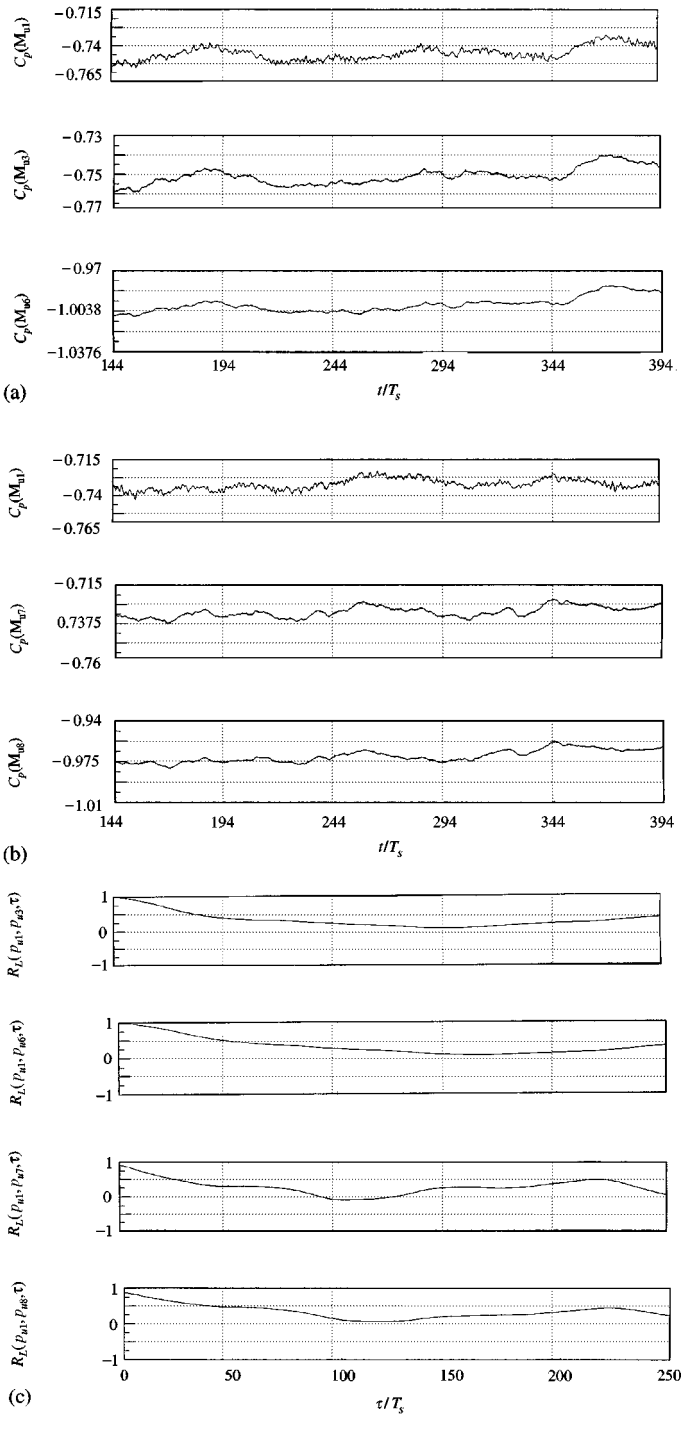

Figure 14. (a) The instantaneous pressure-signal traces obtained at the pressure taps (a) M_{u1}, M_{u3}, and M_{u6} on the circular cylinder, at $Re = 2{\cdot}7 \times 10^4$. (b) The instantaneous pressure-signal traces obtained at the pressure taps (a) M_{u1}, M_{u7}, and M_{u8} on the circular cylinder, at $Re = 2{\cdot}7 \times 10^4$. (c) Plots of $R_L(p_{u1}, p_{u3}, \tau)$, $R_L(p_{u1}, p_{u6}, \tau)$, and $R_L(p_{u1}, p_{u7}, \tau)$, R_L (p_{u1}, p_{u8}, τ) for the low-pass traces corresponding to those shown in Figures 14(a) and 14(b).

In the present work, the low-frequency variations seen in vortex shedding were found to be associated with unsteady variations of the vortex formation length. This finding could complement the previous findings of Lisoski (1993), Szepessy & Bearman (1992) and Roshko (1993) that the low-frequency modulations in vortex shedding are associated with the phase incoherence of vortex-shedding structures in the spanwise direction. Via results obtained by direct numerical simulation for flow over a bluff body subject to the spanwise periodic boundary condition, Henderson (1997) pointed out that the spanwise structures embedded in vortex shedding depend upon the aspect ratio as well as the Reynolds number of the flow. Logically, these findings further motivate an interesting question with regard to the unsteady behaviour of the vortex formation length in the spanwise direction. The answer to this question is unknown at present, and hence this is of interest to be investigated in the future.

ACKNOWLEDGEMENTS

This work was supported by National Science Council, Republic of China, under contract number NSC 85-2622-E-006-018.

References

Bearman, P. W. 1967 The effect of base bleed on the flow behind a two-dimensional model with a blunt trailing edge. *The Aeronautical Quarterly* **18,** 207–224.

Bearman, P. W. 1965 Investigation of the flow behind a two-dimensional model with a blunt trailing edge and fitted with splitter plates. *Journal of Fluid Mechanics* **21,** 241–255.

Blackburn, H. M. & Melbourne, W. H. 1996 The effect of free-stream turbulence on sectional lift forces on a circular cylinder. *Journal of Fluid Mechanics* **306,** 267–292.

Blevins, R. D. 1977 *Flow-Induced Vibration.* New York: Van Nostrand Reinhold.

Bloor, M. S. 1964 The transition to turbulence in the wake of a circular cylinder. *Journal of Fluid Mechanics* **19,** 290–304.

Bloor, M. S. & Gerrard, J. H. 1966 Measurements on turbulent vortices in a cylinder wake. *Proceedings of the Royal Society of London* A**294,** 319–342.

Gerrard, J. H. 1978 The wakes of cylinder bluff body at low Reynolds number. *Philosophical Transactions of the Royal Society of London* A**288,** 351–382.

Goldschmidt, V. W. 1973 Flapping of a plane jet. *Physics of Fluids* **16,** 354–355.

Henderson, R. C. 1997 Nonlinear dynamics and pattern formation in turbulent wake transition. *Journal of Fluid Mechanics* **352,** 65–112.

Kiya, M. & Sasaki, K. 1983 Structure of a turbulent separation bubble. *Journal of Fluid Mechanics* **137,** 83–113.

König, M., Eisonlohr H. & Eckelmann, H. 1990 The fine structure in the Strouhal–Reynolds number relationship of the laminar wake of a circular cylinder. *Physics of Fluids* A**2,** 1607–1614.

Lisoski, D. 1993 Normally two-dimensional flow about a normal flat plate. Ph.D. Thesis, California Institute of Technology, Pasadena, CA, U.S.A.

Miau, J. J., Yang, C. C., Chou, J. H. & Lee, K. R. 1993 Suppression of low-frequency variations in vortex shedding by a splitter plate behind a bluff body. *Journal of Fluids and Structures* **7,** 897–912.

Miau, J. J., Yang, C. C., Chou, J. H. & Lee, K. R. 1993 A t-shaped vortex shedder for a vortex flowmeter. *Flow Measurement and Instruments* **4,** 259–267.

Najjar, F. M., & Balachander, S. 1997 Low-frequency unsteadiness in the wake of a normal flat plate. TAM Report No. 860, UILU-ENG-97-6071, Department of Theoretical and Applied Mechanics, University of Illinois, U.S.A.

Roshko, A. 1954 On the development of turbulent wakes from vortex streets. NACA Report 1191.

Roshko, A. 1993 Perspectives on bluff body aerodynamics. *Journal of Wind Engineering and Industrial Aerodynamics* **49,** 79–100.

Schewe, G. 1983 On the force fluctuations acting on a circular cylinder in crossflow from subcritical up to transcritical Reynolds numbers. *Journal of Fluid Mechanics* **133,** 265–285.

Stäger, R. & Eckelmann, H. 1991 The effect of endplates on the shedding frequency of a circular cylinders in the irregular range. *Physics of Fluids* A **3,** 2116–2121.
Szepessy, S. & Bearman, P. W. 1992 Aspect ratio and end plate effects on vortex shedding from a circular cylinder. *Journal of Fluid Mechanics* **234,** 191–217.
Tanner, M. 1975 Reduction of base drag. *Progress in Aerospace Science* **16,** 369–384.
Unal, M. F. & Rockwell, D. 1988 On vortex formation from a cylinder. Part I. The initial instability. *Journal of Fluid Mechanics* **190,** 491–512.
Wong, H. Y. 1985 Wake flow stabilization by the action of base bleed. *ASME Journal of Fluids Engineering* **107,** 378–384.
Wood, C. J. 1964 The effect of bleed on a periodic wake. *Journal of the Royal Aeronautical Society* **68,** 477–482.